Journal of the Royal Statistical Society Series C: Applied Statistics, 2023, **72**, 1354–1374
https://doi.org/10.1093/jrsssc/qlad060
Advance access publication 3 August 2023
Original Article

ROYAL STATISTICAL SOCIETY DATA | EVIDENCE | DECISIONS
Journal of the Statistics Society
Series C
Applied Statistics

Confidence tubes for curves on SO(3) and identification of subject-specific gait change after kneeling

Fabian J.E. Telschow[1], Michael R. Pierrynowski[2] and Stephan F. Huckemann[3]

[1]Institute of Mathematics, Humboldt Universität zu Berlin, Berlin, Germany
[2]School of Rehabilitation Science, McMaster University, Hamilton, Canada
[3]Felix Bernstein Institute for Mathematical Statistics in the Biosciences, Georgia Augusta University of Göttingen, Göttingen, Germany

Address for correspondence: Fabian J.E. Telschow, Institute of Mathematics, Humboldt Universität zu Berlin, Unter den Linden 6, 10099 Berlin, Germany. Email: fabian.telschow@hu-berlin.de

Abstract

In order to identify changes of gait patterns, e.g. due to prolonged occupational kneeling, which might be a major risk factor for the development of knee osteoarthritis, we develop confidence tubes for curves following a perturbation model on SO(3) using the Gaussian kinematic formula which are equivariant under gait similarities and have precise coverage even for small sample sizes. Applying them to gait curves from eight volunteers undergoing kneeling tasks and adjusting for different walking speeds and marker replacement at different visits, allows us to identify at which phases of the gait cycle the gait pattern changed due to kneeling.

Keywords: functional data analysis, Gaussian kinematic formula, Gaussian perturbation models, Lie groups, modulo group actions, two-sample tests

1 Introduction

There is overwhelming evidence that *prolonged occupational kneeling* (POK), e.g. floor tile laying, constitutes a major risk factor for the development of knee osteoarthritis, e.g. Cooper et al. (1994), Coggon et al. (2000), and Rytter, Egund, et al. (2009). Also, POK is a risk factor for the development of degenerative tears in medial menisci, e.g. Rytter, Jensen, et al. (2009). In order to identify hypothesised underlying changes of gait patterns, kneeling workers' and controls' gait has been compared by Gaudreault et al. (2013) and prolonged kneeling has been *simulated* and gait changes compared by Kajaks and Costigan (2015) and L. M. Tennant et al. (2018). Also, dependence of kneeling effects due to footwear has been investigated by L. Tennant et al. (2015) and kneeling effects have been studied on cadavers with total knee arthroplasty (Wilkens et al., 2007).

In order to assess the specifics of changes of gait patterns, the three-dimensional rotational path in SO(3) of the relative motion of the tibia (larger lower leg bone) w.r.t. the femur (upper leg bone) is usually represented by the three Euler angles flexion/extension, adduction/abduction, and internal/external rotation. This is the output experimenters get from proprietary camera systems such as *Plug-In Gait* (Vicon, Oxford Metrics, London, UK). Using the relative motions, Gaudreault et al. (2013), Kajaks and Costigan (2015), and L. M. Tennant et al. (2018) have found, among others, for each angle, loci of significant gait changes, without, however, addressing the issue of multiple testing, correlation of the sequential data, and the effect of marker replacement.

In our approach, we address all of these issues, and in consequence, are able to test for subject-specific changes of gait pattern. In application, we do this for pre- and post-kneeling, the method,

Received: October 1, 2021. **Revised:** January 6, 2023. **Accepted:** June 14, 2023

however, is applicable for any change of condition (e.g. onset of otheoathritis) over a period of time, in particular it corrects for marker replacement. To this end, we recall a Gaussian perturbation model from Telschow et al. (2020) for curves on Lie groups, apply it to SO(3) and build an oracle simultaneous confidence tube (SCT) for the centre curve (Theorem 3.4). We call it an oracle SCT, since the unknown quantile to calibrate the covering of the SCT depends on the true centre curve and therefore cannot be computed immediately. Building on the work (Rancourt et al., 2000), assuming that the variance of the error process in the Gaussian perturbation (GP) model is small, we show that the unknown quantile can be approximated by the quantiles of an Hotelling statistic and that the unknown quantile can be estimated by the *Gaussian kinematic formula* (GKF), see J. E. Taylor (2006) and J. Taylor and Worsley (2008). An important feature of the developed SCTs is that they are equivariant with respect to the group action describing the marker replacement and the different walking speeds (Theorem 3.6).

In application to gait analysis, our method, relying on curves on the rotational group, takes advantage of simultaneously involving all three Euler angles in a canonical way and can be motivated by the actual data generation (Section 5). Moreover, as the multiple testing issue is resolved by providing SCTs over entire gait cycles, the sequential correlation is naturally modelled within the GKF approach, the SCTs are equivariant with respect to the effect of marker replacements, which is important in our application to gait analysis (Section 5), and our simulations mimicking and going beyond the use case of low variance and high smoothness typical in gait analysis show that our approximations of the oracle SCTs have precise covering rates even for small sample sizes (Section 4), our SCTs are well applicable in gait analysis.

We report their application to an experiment conducted in the School of Rehabilitation Science at McMaster University (Canada) in Section 5. Here, we can identify for six out of eight healthy volunteers changes of their gait patterns after kneeling tasks by identifying time points where the SCTs do not overlap. We find that after kneeling, deviation from normal gait is stronger, in particular for older aged male volunteers. Our analysis also involves correcting for different walking speeds and marker replacement, at a subsequent patient's visit, since it is well known that Euler angle curves may change considerably after marker replacement and simple approaches subtracting average angles over gait cycles (cf. Kadaba et al., 1989) have remained questionable, e.g. Delval et al. (2008), McGinley et al. (2009), Noehren et al. (2010), and Røislien et al. (2012). This has lead to the longstanding open problem of *gait reproducibility*, see Duhamel et al. (2004). We also explain in detail the effect of the marker replacement on the observed relative rotation curves and use the method, which we developed in a recent publication (Telschow et al., 2020), to correct for this effect. The main challenge here is that the proprietary software reports only the Euler angles of the observed relative rotations of the knee joint. Since volunteers will have different comfortable walking speeds at different visits, we also have corrected for this sample-specific time warping effect using the methodology described in Telschow et al. (2020).

The biomechanical gait analysis tool chain developed in this contribution, sketched in Figure 1, is available under www.stochastik.math.uni-goettingen.de/KneeMotionAnalytics as an R-package, including all data and code used in this paper.

2 Gaussian perturbation models on SO(3)

The Lie group $\mathrm{SO}(3) = \{R \in \mathbb{R}^{3\times 3} : R^T = R^{-1},\ \det(R) = 1\}$ comes with the Lie algebra $\mathfrak{so}(3) = \{A \in \mathbb{R}^{3\times 3} : A^T = -A\}$ of 3×3 skew symmetric matrices which is isomorphic to $\mathbb{R}^3$ by the map $\imath : \mathbb{R}^3 \to \mathfrak{so}(3)$ given by

$$\imath(a) = \begin{pmatrix} 0 & -a_3 & a_2 \\ a_3 & 0 & -a_1 \\ -a_2 & a_1 & 0 \end{pmatrix}$$

for $a = (a_1, a_2, a_3)^T \in \mathbb{R}^3$. The isomorphism $\imath$ satisfies the following useful relation:

$$Q\imath(a)Q^T = \imath(Qa) \text{ for all } a \in \mathbb{R}^3 \text{ and } Q \in \mathrm{SO}(3). \tag{1}$$

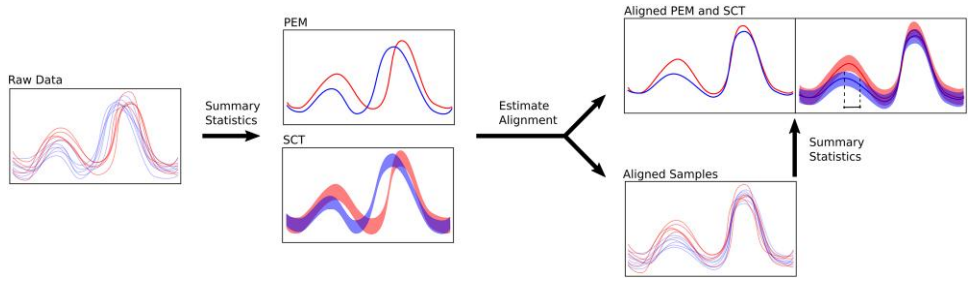

Figure 1. Exemplifying one Euler angle from our tool chain to compare two samples of three-dimensional rotatonal curves. The two samples and their corresponding measures are have different colors (red and blue). The left panel shows the raw data, while the middle panel visualizes the point-wise extrinsic mean (PEM) curves. The spatio-temporal aligned PEMs, samples and the corresponding simultaneous confidence tubes (SCT) are found in the third panel. Here the non-overlap of the SCT which indicates significant deviation of the gait pattern is highlighted by a black interval with end points being the black dashed lines.

On $\mathbb{R}^{3\times3}$ we use the scalar product $\langle A, B\rangle := \mathrm{trace}(AB^T)/2$ which induces the rescaled Frobenius norm $\|A\|_F = \sqrt{\mathrm{trace}(AA^T)/2} = \|a\|$ on $\mathbb{R}^{3\times3}$ and satisfies $\langle A, B\rangle = a^T b$for $A, B \in \mathfrak{so}(3)$with $\iota^{-1}(A) = a$and $\iota^{-1}(B) = b$.

As usual, the unit matrix will be denoted with $I_{3\times3}$and $A \mapsto \mathrm{Exp}(A)$denotes the matrix exponential which is identical to the Lie exponential of SO(3)and gives a surjection $\mathfrak{so}(3) \to \mathrm{SO}(3)$. Due to skew symmetry, the matrix exponential satisfies the so-called *Rodriguez formula*, i.e.

$$\mathrm{Exp}(A) = I_{3\times3} + \frac{\sin(\|A\|_F)}{\|A\|_F} A + \frac{1-\cos(\|A\|_F)}{\|A\|_F^2} A^2, \tag{2}$$

which shows that Expis bijective on $\mathcal{B}_\pi(0) = \{A \in \mathfrak{so}(3) : \|A\|_F < \pi\}$, compare Chirikjian (2000, p. 121) for further details.

For $I = [0, 1]$, we denote with $\Gamma = \mathcal{C}^p(I, G)$, $p \in \mathbb{N}$, the space of p times continuously differentiable curves on SO(3). As in Telschow et al. (2020), we assume that the observed SO(3)-valued curves are generated by the following Gaussian perturbation model.

Definition 2.1 We say that a random curve $\gamma \in \Gamma$follows a *GP* around a *centre curve* $\gamma_0 \in \Gamma$if there is an $\mathbb{R}^3$-valued zero-mean Gaussian process $a_t$with almost surely $\mathcal{C}^p$paths such that

$$\gamma(t) = \gamma_0(t)\mathrm{Exp}\big(\iota(a_t)\big) \tag{3}$$

for all $t \in I$. The Gaussian process $a_t$will be called the *generating process*.

This model, which is based on right multiplication with the exponential of the generating process is equivalent to a model based on left multiplication and asymptotically (as the variance goes to zero) equivalent to a model based on two-sided multiplication, cf. Telschow et al. (2020). Moreover, it is invariant under the *spatial* action of $\mathrm{SO}(3) \times \mathrm{SO}(3)$on Γ given point-wise by $(Q, P) \circ \gamma(t) = Q\gamma(t)P$, $t \in I$, and under the temporal action

$$\phi \in \mathrm{Diff}^+(\mathrm{I}) = \{\phi \in \mathcal{C}^\infty(\mathrm{I}, \mathrm{I}) : \phi'(\mathrm{t}) > 0 \text{ for all } \mathrm{t} \in \mathrm{I}\}$$

of strictly monotone time warpings. We call $\mathcal{S} = (\mathrm{SO}(3) \times \mathrm{SO}(3)) \times \mathrm{Diff}^+(\mathrm{I})$the space of gait similarities and write $(\psi, \phi) \circ \gamma = \psi \circ \gamma \circ \phi$for the corresponding action on Γ which is defined by $(\psi \circ \gamma \circ \phi)(t) = \psi(\gamma(\phi(t)))$for all $t \in I$.

For independent i.i.d. samples $\chi_1 = \{\gamma_1, \ldots, \gamma_N\}$and $\chi_2 = \{\eta_1, \ldots, \eta_M\}$, $N, M \in \mathbb{N}$, of GP models γ and η with centre curves $\gamma_0$and η_0, respectively, we have developed in Telschow et al. (2020) a

two-sample rank permutation tests for the hypotheses

$$H_0: \quad \exists(\psi, \phi) \in \mathcal{S}: \gamma \sim \psi \circ \eta \circ \phi \quad \text{vs.} \quad H_1: \quad \forall(\psi, \phi) \in \mathcal{S}: \gamma \not\sim \psi \circ \eta \circ \phi \tag{4}$$

at a given significance level $\alpha \in (0, 1)$. In contrast to classical shape analysis which corrects for a group action on individual measurements, this test corrects for a common *sample-specific group action*. Since this test is a global test, it cannot identify time points at which the centre curves $\gamma_0$and $\eta_0$of the tested samples differ, it only indicates whether the samples come from the same GP model up to the group action of $\mathcal{S}$on Γ.

3 Confidence tubes for centre curves of GP models on SO(3)

In applications such as the biomechanical data presented in Section 5, which studies the effect of a kneeling intervention on the gait pattern of different subjects, it is often of interest to identify at which time points the centre curves of two samples differ. In order to achieve this, we now construct an SCT for $\gamma_0$in a GP model on SO(3).

As in Telschow et al. (2020), we estimate $\gamma_0$by the *point-wise extrinsic mean* (PEM) curve $\hat{\gamma}_N(t)$of a sample $\gamma_1, \ldots, \gamma_N \overset{\text{i.i.d.}}{\sim} \gamma \in \Gamma$which is defined for each $t \in [0, 1]$by

$$\hat{\gamma}_N(t) \in \hat{E}_N(t) = \operatorname*{argmin}_{\mu \in \mathrm{SO}(3)} \frac{1}{N} \sum_{n=1}^{N} \|\mu - \gamma_n(t)\|_F^2. \tag{5}$$

It computes the PEM, cf. Bhattacharya and Patrangenaru (2003), of $\mathrm{SO}(3) \subset \mathbb{R}^3$with respect to the norm $\|\cdot\|_F$. The PEM fulfils the following uniqueness and convergence properties for GP models proven in Telschow et al. (2020).

Theorem 3.1 Let $\gamma_1, \ldots, \gamma_N$be a sample of a random curve $\gamma \in \Gamma$following a GP model around a centre curve $\gamma_0$and let $t \mapsto \hat{\gamma}_N(t)$be a measurable selection of $\hat{E}_N(t)$for each time point $t \in I$. If the generating Gaussian process $a_t$satisfies

$$\mathbb{E}\left[\max_{t \in [0,1]} \|\partial_t \iota(a_t)\|_F\right] < \infty, \tag{6}$$

then the following hold:

(i) There is $\Omega' \subset \Omega$measurable with $\mathbb{P}(\Omega') = 1$such that for every $\omega \in \Omega'$there is $N_\omega \in \mathbb{N}$such that for all $N \geq N_\omega$, every $\hat{E}_N(t)$has a unique element $\hat{\gamma}_N(t)$for all $t \in I$and $\hat{\gamma}_N \in \Gamma$;
(ii) $\max_{t \in [0,1]} \|\hat{\gamma}_N(t) - \gamma_0(t)\|_F \to 0$for $N \to \infty$almost surely.

Corollary 3.2 With the notations and assumptions of Theorem 3.1, we have

$$\lim_{N \to \infty} \mathbb{P}\left\{t \mapsto \hat{\gamma}_N(t) \in \Gamma\right\} = 1.$$

The inverse of the Lie exponential Expis well defined on $\mathrm{Exp}(\mathcal{B}_\pi(0))$and, since the Lie exponential is a surjection, its inverse on $\mathrm{Exp}(\mathcal{B}_\pi(0))$can be extended to a bijective, right inverse $\mathrm{Log}: \mathrm{SO}(3) \to \mathfrak{so}(3)$which is continuous on $\mathrm{Exp}(\mathcal{B}_\pi(0))$but has discontinuities on $\mathrm{SO}(3) \setminus \mathrm{Exp}(\mathcal{B}_\pi(0))$.

Definition 3.3 Let $\gamma_1, \ldots, \gamma_N$be a sample of a random curve $\gamma \in \Gamma$following a GP model around a centre curve $\gamma_0$and let $\hat{\gamma}_N$be an estimator for $\gamma_0$and $\mathfrak{L} = \iota^{-1} \circ \mathrm{Log}$. Then

$$x_t^N = \mathfrak{L}\big(\hat{\gamma}_N^{-1}(t)\gamma_0(t)\big) \quad \text{and} \quad x_t^{N,n} = \mathfrak{L}\big(\hat{\gamma}_N^{-1}(t)\gamma_n(t)\big)$$

are called *intrinsic population* and *sample residuals*, respectively.

If we assume that the sample covariance matrix $\hat{S}_t^x = (N-1)^{-1}\sum_{n=1}^N x_t^{N,n}(x_t^{N,n})^T$ derived from the sample residuals is non-singular for all $t \in I$, we can define the one-dimensional *oracle process*

$$\hat{H}_t^x = N\left(x_t^N\right)^T\left(\hat{S}_t^x\right)^{-1}x_t^N, \tag{7}$$

as it is not directly observable, since it depends on γ_0. Nevertheless, it allows us to construct simultaneous $(1-\alpha)$confidence tubes for $\gamma_0$stated in our next theorem by introducing for any $\alpha \in (0, 1)$the quantile

$$\hat{h}_{\gamma_0,N,\alpha} = \inf\left\{h \in \mathbb{R} \mid \mathbb{P}\left\{\sup_{t\in I}\hat{H}_t^x \le h\right\} \ge 1-\alpha\right\}$$

and the set

$$\mathcal{V}_\alpha(\gamma_1, \ldots, \gamma_N; t) = \left\{a \in \mathbb{R}^m \mid Na^T\left(\hat{S}_t^x\right)^{-1}a \le \hat{h}_{\gamma_0,N,\alpha}\right\}.$$

Theorem 3.4 (Oracle Confidence Tubes). Let $\gamma_1, \ldots, \gamma_N$be a sample of a random curve $\gamma \in \Gamma$following a GP model around a centre curve γ_0. Let $\hat{\gamma}_N$be an estimator for $\gamma_0$and assume $\hat{S}_t^x$to be non-singular for all $t \in I$. Then

$$\mathbb{P}\left\{\gamma_0(t) \in \hat{\gamma}_N(t)\mathrm{Exp}(\iota(\mathcal{V}_\alpha(\gamma_1, \ldots, \gamma_N; t))) \text{ for all } t \in I\right\} \ge 1-\alpha.$$

The process $\hat{H}_t^x$from equation (7) depends on $\gamma_0$and therefore the quantile $\hat{h}_{\gamma_0,N,\alpha}$is not directly computable. Using ideas from Rancourt et al. (2000) and extending them to Gaussian processes, we show in the next section for observations $\gamma_n(t) = \gamma_0\mathrm{Exp}(\iota(a_t)^n)$for $1 \le n \le N$, $t \in I$and $\mathbb{E}[\iota(a_t^n)] = 0$, and σ small enough that the process $\hat{H}_t^x$can be approximated by the *genuine Hotelling process* obtained from the generating process of the GP model, i.e.

$$H_t^a = N\bar{a}_t^T\left(S_t^a\right)^{-1}\bar{a}_t, \tag{8}$$

with

$$\bar{a}_t = \frac{1}{N}\sum_{n=1}^N a_t^n, \quad S_t^a = \frac{1}{N-1}\sum_{n=1}^M\left(a_t^n - \bar{a}_t\right)\left(a_t^n - \bar{a}_t\right)^T. \tag{9}$$

Remark 3.5 At first glance, this approximation seems not helpful, since the process $H_t^a$is not observable either. The benefit though is that it has a Hotelling T^2-distribution for each $t \in I$. Therefore, the quantiles of the maximum over I of H_t^acan be approximated using the Gaussian kinematic formula or bootstraps based on the observed residuals $x_t^{N,n}$if the maximal variance along $\gamma(t)$is sufficiently small compared to the injectivity radius of $SO(3)$as will be discussed in the next section.

Our next theorem establishes the equivariance property of the SCTs with respect to the group action of $\mathcal{S}$on Γ.

Theorem 3.6 Let $\gamma_1, \ldots, \gamma_N$be a sample of a random curve $\gamma \in \Gamma$following a GP model around a centre curve $\gamma_0$with PEM curve $\hat{\gamma}_N$. Moreover, let $(\psi, \phi) = ((P_\psi, Q_\psi), \phi) \in \mathcal{S}$be arbitrary, acting on Γ point-wise by $(\psi \circ \gamma \circ \phi)(t) = P_\psi \gamma(\varphi(t)) Q_\psi$, $t \in I$and define the sample $\eta_n = \psi \circ \gamma_n \circ \phi$, $n \in \{1, \ldots, N\}$of the GP $\psi \circ \gamma \circ \phi$with centre curve $\eta_0 = \psi \circ \gamma_0 \circ \phi$and PEM curve $\hat{\eta}_N$. Then, for every $0 \leq \alpha \leq 1$, the SCTs for $\psi \circ \gamma_0 \circ \phi$computed from $\eta_1, \ldots, \eta_N$satisfy

$$\hat{\eta}_N(t)\mathrm{Exp}\big(\iota\big(\mathcal{V}_\alpha(\eta_1, \ldots, \eta_N; t)\big)\big) = (\psi \circ \hat{\gamma}_N \circ \phi)(t)\mathrm{Exp}\big(\iota\big(Q_\psi \mathcal{V}_\alpha(\gamma_1, \ldots, \gamma_N; \phi(t))\big)\big),$$

i.e. they can be derived from the SCTs for $\gamma_0$using only $\gamma_1, \ldots, \gamma_N$and $(\psi, \phi) \in \mathcal{S}$.

3.1 Approximating confidence tubes on SO(3)

The main result of this section is that the residual processes $x_t^N$and $x_t^{N,n}$from Definition 3.3 are in the case of concentrated errors approximately the residuals of the generating Gaussian process (9) of the GP model. This implies, in particular, that for concentrated errors the unobservable process $\hat{H}_t^x$is approximately a Hotelling T^2process. Making such concentrated error approximations is justified in biomechanics, since the generating error process $a_t$of the error in the movements of the joints is usually small compared to the injectivity radius of SO(3), compare also Section 5 for an explanation of the physical source of the error process. Rancourt et al. (2000) used the same 'small variance' approximation and our result can be viewed as an extension of their results to random curves. In particular, an inspection of our proof of the next theorem reveals that it does not require that the generating process in the Lie algebra is Gaussian.

Theorem 3.7 (Approximations for Concentrated Errors). Let $N \in \mathbb{N}$be fixed and $\gamma_1, \ldots, \gamma_N$be a sample of a random curve $\gamma \in \Gamma$following a GP model around a centre curve γ_0. Additionally, assume that the generating Gaussian process $a_t$satisfies $\mathbb{E}[\max_{t \in I} \|\iota(\partial_t a_t)\|_F] < \infty$and $\max_{t \in I} \|\iota(a_t)\|_F = \mathcal{O}_p(\sigma)$with $0 < \sigma \to 0$. Let $\hat{\gamma}_N(t)$be a measurable selection of sample PEM curves. Then, for $x_t^N$and $x_t^{N,n}$from Definition 3.3 it holds

$$x_t^N = \bar{a}_t + \mathcal{O}_p\big(\sigma^2\big), \quad x_t^{N,n} = a_t^n - \bar{a}_t + \mathcal{O}_p\big(\sigma^2\big), \tag{10}$$

where $\mathcal{O}_p(\sigma^2)$is uniform over I.

Corollary 3.8 (Asymptotically genuine Hotelling process). Under the assumptions and notations of Theorem 3.7 and assuming $\mathrm{cov}[a_t] = \sigma^2 \Sigma_t$with a non-singular $\Sigma_t$for all $t \in I$, we have that $H_t^a = \hat{H}_t^x + \mathcal{O}_p(\sigma)$, where $\mathcal{O}_p(\sigma)$holds uniformly over I.

By the above corollary, the process H_t^awhich is Hotelling-$T_{3,N-1}$-distributed is approximately equal to the oracle process $\hat{H}_t^x$for small σ. The intuition is that if the variance of the process is not too large, then all sample paths $\hat{\gamma}_N^{-1}(t)\gamma_0(t)$and $\hat{\gamma}_N^{-1}(t)\gamma_n(t)$, $n \in \{1, \ldots, N\}$, are with high probability completely contained in $\mathrm{Exp}(\mathcal{B}_\pi(0))$and therefore the discontinuity of $\mathfrak{L}$on the boundary does not cause problems when inverting to get the residuals.

3.1.1 The GKF

Corollary 3.8 states that for concentrated errors, the statistic H_t^a, which is the Hotelling T^2statistic of a sample of size N of the generating Gaussian process a, approximates the oracle statistic $\hat{H}_t^x$, cf. Remark 3.5. Thus, in order to estimate the quantiles $\hat{h}_{\gamma_0,N,\alpha}$for the process $\hat{H}_t^x$, derived from a GP model γ, we use the *expected Euler characteristic (EC) heuristic*, for example, J. Taylor et al.

(2005), i.e. that for $h > 0$large enough the following approximate identity holds:

$$\mathbb{P}\left(\max_{t\in I} \hat{H}_t^x > h\right) \approx \mathbb{E}\left[\mathfrak{x}\left(\left\{t \in I | \hat{H}_t^x \geq h\right\}\right)\right] \approx \mathbb{E}\left[\mathfrak{x}\left(\left\{t \in I | H_t^a \geq h\right\}\right)\right]. \tag{11}$$

Here, $\mathfrak{x}(\mathcal{U})$denotes the *EC* of $\mathcal{U} \subseteq I$. Although we cannot rigorously justify this approximation, our simulations in Section 4 show that this procedure works very well even for small sample sizes.

Under the assumption that the generating Gaussian process $a_t$has $\mathcal{C}^2$-sample paths and some additional weak technical assumptions given in J. E. Taylor (2006), it is shown in J. Taylor and Worsley (2008) that the expected EC of the excursion set $\{t \in I \mid H_t^a \geq h\}$can be computed explicitly by the formula

$$\mathbb{E}\left[\mathfrak{x}\left(\left\{t \in I \mid H_t^a \geq h\right\}\right)\right] = \rho_0(h) + \mathcal{L}_1[a_t]\rho_1(h). \tag{12}$$

Here, the so-called *Lipschitz-Killing curvature* $\mathcal{L}_1[a_t]$is given by the functional

$$\mathcal{L}_1[a_t] = \int_0^1 \sqrt{\operatorname{var}\left[\frac{\mathrm{d}a}{\mathrm{d}t}(t)\right]}\,\mathrm{d}t,$$

with $a_t$being the generating Gaussian process of the GP model. Moreover, the *Euler characteristic densities* ρ_j, $j \in \{0, 1\}$, of a $T_{3,N-1}$process appearing in the GKF (12) can be computed from the EC densities of a Students t_{N-1}-process via Roy's union intersection principle [cf. J. Taylor and Worsley (2008, Section 3.1)] resulting in the formula

$$\rho_j(h) = \sum_{d=0}^{3} \mu_d(S^2)\rho_{j+d}^s\left(\sqrt{h}\right), \quad j = 0, 1.$$

Here, $\mu_d(S^2)$denotes the d-dimensional intrinsic volume of the two-sphere S^2

$$\mu_0(S^2) = 2, \quad \mu_1(S^2) = 0, \quad \mu_2(S^2) = 4\pi, \quad \mu_3(S^2) = 0$$

as in J. Taylor and Worsley (2008, p. 23), recalling that the Hotelling process can be viewed as living on S^2, since we divide by the variance. In relation to Stochastic Geometry literature [e.g. Mecke and Stoyan (2000, p. 100)], $\mu_0$gives twice the number of connected components and $\mu_2$gives the surface area of S^2. Moreover, the EC densities of a random process with Student's t_{N-1}distributed marginals have the explicit representations

$$\rho_0^s(h) = \int_h^\infty \frac{\Gamma\left(\frac{N}{2}\right)}{\sqrt{N-1}\pi\Gamma\left(\frac{N-1}{2}\right)}\left(1 + \frac{u^2}{N-1}\right)^{-N/2} du$$

$$\rho_1^s(h) = (2\pi)^{-1}\left(1 + \frac{h^2}{N-1}\right)^{1-N/2}$$

$$\rho_2^s(h) = (2\pi)^{-3/2}\frac{\Gamma\left(\frac{N}{2}\right)}{\sqrt{\frac{N-1}{2}}\Gamma\left(\frac{N-1}{2}\right)} h\left(1 + \frac{h^2}{N-1}\right)^{1-N/2}$$

$$\rho_3^s(h) = (2\pi)^{-2}\left(\frac{N-2}{N-1}h^2 - 1\right)\left(1 + \frac{h^2}{N-1}\right)^{1-N/2},$$

given in J. E. Taylor and Worsley (2007, p. 915).

3.1.2 Estimation of the quantile

Using the GKF for Hotelling T^2-processes together with the EC heuristic (11) yields

$$\mathbb{P}\left(\max_{t\in I}\hat{H}_t^x > h\right) \approx 2\rho_0^s(\sqrt{h}) - 4\pi\rho_2^s(\sqrt{h}) - \mathcal{L}_1[a_t]\left(2\rho_1^s(\sqrt{h}) + 4\pi\rho_3^s(\sqrt{h})\right),$$

which could be used to approximate the value $\hat{h}_{\gamma_0,N,\alpha}$for low probabilities α if $\mathcal{L}_1[a_t]$is known by solving

$$2\rho_0^s\left(\sqrt{h}\right) - 4\pi\rho_2^s\left(\sqrt{h}\right) - \mathcal{L}_1[a_t]\left(2\rho_1^s\left(\sqrt{h}\right) + 4\pi\rho_3^s\left(\sqrt{h}\right)\right) = 1-\alpha. \tag{13}$$

Thus, it remains to estimate $\mathcal{L}_1[a_t]$. This has been achieved for Gaussian processes in $\mathbb{R}^D$, $D \in \mathbb{N}$, in J. E. Taylor and Worsley (2007, Section 4) and J. Taylor and Worsley (2008), where they also proved that their estimator is consistent. Since the estimator of J. Taylor and Worsley (2008, equation (18)) is based only on the Gaussian residuals, we adapt their estimator by replacing their residuals by the intrinsic residuals to obtain an estimator of $\mathcal{L}_1[a_t]$. This is justified, since the intrinsic residuals of a sample from a GP model γ are, in case of concentrated errors, close to the residuals of the generating Gaussian process $A_t = \imath(a_t)$by Theorem 3.7. For convenience we state the resulting estimator explicitly.

Let $\gamma_1, \ldots, \gamma_N$be a sample of a GP model γ and assume the curves are observed at times $0 = t_1 < t_2 < \cdots < t_K = 1$. Using the $x_t^{N,n}$from Definition 3.3, we define the matrix

$$R_{t_k} = \left(x_{t_k}^{N,n}, \ldots, x_{t_k}^{N,n}\right)^T \in \mathbb{R}^{N\times 3}$$

and denote with $R_{t_k}^d$the dth column of R_{t_k}. The normalised residuals are given by $\hat{R}_{t_k}^d = R_{t_k}^d / \|R_{t_k}^d\|$for $d \in \{1, 2, 3\}$and $k \in \{1, \ldots, K\}$. The estimator of $\mathcal{L}_1$is then given by

$$\widehat{\mathcal{L}_1[a_t]} = \frac{1}{3}\sum_{k=1}^{K-1}\sum_{d=1}^{3}\left\|\hat{R}_{t_{k+1}}^d - \hat{R}_{t_k}^d\right\|. \tag{14}$$

4 Simulations of covering rates

In this section, we study the actual covering rate of the proposed SCTs' construction which is based on approximating the quantile $\hat{h}_{\gamma_0,N,\alpha}$for concentrated error processes.

4.1 GP models used for simulation

Without loss of generality we may assume that our centre curves satisfy $\gamma_0(t) = I_{3\times 3}$for all $t \in I$, since we can multiply the sample with $\gamma_0(t)^{-1}$from the left and use Theorem 3.6. In our simulations, we construct the generating Gaussian process for the used GP models from the error processes

$$\begin{aligned}
\varepsilon_t^{1,l} &= f_l(t)\left(b_1 \sin\left(\frac{\pi}{2}t\right) + b_2\cos\left(\frac{\pi}{2}t\right)\right)\\
\varepsilon_t^{2,l} &= f_l(t)\left(\frac{\sum_{i=1}^{10} b_i e^{-\frac{\left(t-\frac{i-1}{9}\right)^2}{0.2}}}{\sqrt{\sum_{i=1}^{10} e^{-2\frac{\left(t-\frac{i-1}{9}\right)^2}{0.2}}}}\right)\\
\varepsilon_t^{3,l} &= f_l(t)\left(b_0 e^{-5t} + \sqrt{10}\int_0^t e^{5(s-t)}dW_t\right)
\end{aligned} \tag{15}$$

with i.i.d. $b_i \sim \mathcal{N}(0, 1)$for $i \in \{0, \ldots, 10\}$, $\{W_t\}_{t\in I}$a Wiener process, and for $l \in \{1, 2, 3\}$we set

$$f_1(t) = 1, \quad f_2(t) = 4, \quad f_3(t) = \sin(4\pi t) + 1.5.$$

These processes satisfy $\mathrm{var}[\varepsilon_t^{v,l}] = f_l(t)^2$for all $t \in I$, $l \in \{1, 2, 3\}$and $v \in \{1, 2, 3\}$. Furthermore, the sample paths of the processes $\varepsilon^{1,l}$and $\varepsilon^{2,l}$have $\mathcal{C}^\infty$sample paths, whereas the sample paths of $\varepsilon^{3,l}$, which is a Ornstein-Uhlenbeck process [e.g. (Iacus, 2009, p. 43)], are only continuous, which implies that the GKF is not applicable for this process. In our simulations, we use

$$A_t^{i,l,j,\sigma} = \iota\left(M_j\left(\sigma\varepsilon_{1,t}^{i,l}, \sigma\varepsilon_{2,t}^{i,l}, \sigma\varepsilon_{3,t}^{i,l}\right)^T\right), \tag{16}$$

for $i \in \{1, 2, 3\}$, $j \in \{1, 2\}$, $l \in \{1, 2, 3\}$, and $\sigma \in \mathbb{R}_{>0}$as the generating Gaussian process $A_t = \iota(a_t)$for our GP models. Here, we denote with $\varepsilon_{s,t}^{i,l}$for $s = 1, 2, 3$independent realisations of the processes $\varepsilon_t^{i,l}$. The matrices

$$M_1 = \begin{pmatrix} 1 & 0 & 0 \\ 0 & 1 & 0 \\ 0 & 0 & 1 \end{pmatrix}, \quad M_2 = \begin{pmatrix} 1 & 0 & 0 \\ \frac{1}{2} & \frac{1}{2} & 0 \\ \frac{1}{\sqrt{3}} & \frac{1}{\sqrt{3}} & \frac{1}{\sqrt{3}} \end{pmatrix}.$$

are introduced to include correlations among the coordinates. Moreover, equation (16) introduces different variances in the coordinates, since for $j = 2$the second component has half the variance of the other two components.

4.2 Design of simulation of SCTs for centre curves of GP models

First, $N \in \{10, 15, 30\}$realisations of the process $A_t^{i,l,j,\sigma}$on the equidistant time grid $\mathcal{T}$with $\Delta t = 0.01$of I for $i \in \{1, 2, 3\}$, $j \in \{1, 2\}$, $l \in \{1, 2, 3\}$, and $\sigma \in \{0.05, 0.1, 0.6\}$are simulated. We only report small sample sizes here, since the asymptotic behaviour has been studied intensely in Telschow and Schwartzman (2022) and small simulation studies for higher sample sizes did not reveal departures from correct covering rates.

For a sample of a GP model, we construct $(1 - \alpha)$-SCT using Theorem 3.4 and estimate the quantile $\hat{h}_{\gamma_0,N,\alpha}$by equation (13) using the Lipschitz-Killing curvature estimator (14). Afterwards it is checked whether $\gamma_0 \equiv I_{3\times 3}$is contained in the SCT for all $t \in \mathcal{T}$. This procedure is repeated $M = 5{,}000$times. The true covering rate is approximated by the relative frequency of the numbers of simulations, in which the constructed SCT contained the true centre curve $\gamma_0$for all $t \in \mathcal{T}$.

4.3 Results of simulation of SCT for centre curves of GP models

The results are reported in Table 1 and they convey a positive message: For a variance $\sigma = 0.05$, which is that of the data of the application in Section 5, the simulated covering rate is very close to $1 - \alpha$. The covering rates are only for the Ornstein-Uhlenbeck error process slightly too high. For higher variance ($\sigma = 0.6$), we underestimate the covering rate. This is expected, since the proposed estimator is designed for concentrated data and the map $v \mapsto \mathrm{Log}(\mathrm{Exp}(v))$is only the identity on $\|v\| < \pi$and we have the inequality

$$\left\|\mathrm{Log}\left(\mathrm{Exp}\left(\iota(v)\right)\right)\right\|_F \leq \|v\|. \tag{17}$$

This implies that our estimated covariance matrix has smaller eigenvalues then the covariance matrix of the sample and hence our confidence sets will become smaller. This effect is more visible if the sample size is large, since more curves cross the cut locus.

5 Application: assessing kneeling effects on gait

5.1 Study design

In a study conducted at the School of Rehabilitation Science (McMaster University, Canada), 8 volunteers (4 female, 4 male, for each gender, two aged 20–30 and two aged 50–60) with no previous knee injuries (external observation and subjective questioning revealed no obvious knee problems) with unremarkable knee kinematics motion have been selected. In the experiment retro-reflective

Table 1. Simulated covering rates (right box) of simultaneous $(1-\alpha)$confidence tubes for Gaussian perturbation models obtained from $M = 5,000$simulations for varying error processes (EP)

N	σ	EP	$1-\alpha$	$i=1$	$i=2$	$i=3$
10	0.05	$A^{i,1,1,\sigma}$	85/90/95	86.1/91.0/95.0	85.3/90.1/95.6	90.4/93.9/96.6
15	0.05	$A^{i,1,1,\sigma}$	85/90/95	85.0/90.1/95.4	85.7/90.7/94.9	89.4/93.0/96.6
30	0.05	$A^{i,1,1,\sigma}$	85/90/95	85.1/91.0/94.9	86.4/90.6/94.7	90.1/93.5/96.5
10	0.05	$A^{i,1,2,\sigma}$	85/90/95	85.3/89.9/94.6	86.1/90.9/95.4	90.1/93.1/97.2
15	0.05	$A^{i,1,2,\sigma}$	85/90/95	85.4/89.8/95.4	85.9/90.5/94.9	90.3/93.0/96.7
30	0.05	$A^{i,1,2,\sigma}$	85/90/95	85.0/90.2/95.6	85.9/89.8/94.9	90.2/92.9/96.6
10	0.05	$A^{i,3,1,\sigma}$	85/90/95	84.8/90.0/95.3	86.2/90.9/95.5	91.0/93.6/97.1
15	0.05	$A^{i,3,1,\sigma}$	85/90/95	84.3/89.9/95.2	86.2/90.6/95.0	90.3/93.0/96.2
30	0.05	$A^{i,3,1,\sigma}$	85/90/95	84.7/90.1/95.2	86.6/90.8/94.9	90.0/92.6/96.5
10	0.05	$A^{i,3,2,\sigma}$	85/90/95	86.0/90.6/95.0	85.4/90.3/95.5	90.3/93.3/96.9
15	0.05	$A^{i,3,2,\sigma}$	85/90/95	84.9/90.0/94.7	85.4/90.5/95.3	90.1/93.5/97.3
30	0.05	$A^{i,3,2,\sigma}$	85/90/95	85.1/89.7/95.3	85.9/90.7/94.9	89.9/92.9/96.5
10	0.1	$A^{i,1,1,\sigma}$	85/90/95	84.7/90.8/94.9	85.2/91.4/95.4	90.3/93.4/96.7
15	0.1	$A^{i,1,1,\sigma}$	85/90/95	84.9/89.8/95.1	86.1/90.4/95.1	89.5/91.6/96.6
30	0.1	$A^{i,1,1,\sigma}$	85/90/95	85.0/90.5/95.1	85.8/91.1/95.5	89.9/92.7/96.3
10	0.1	$A^{i,1,2,\sigma}$	85/90/95	85.5/90.4/94.5	86.3/90.8/95.1	90.3/93.3/96.4
15	0.1	$A^{i,1,2,\sigma}$	85/90/95	85.4/89.9/94.7	86.1/89.9/95.3	89.9/93.1/95.9
30	0.1	$A^{i,1,2,\sigma}$	85/90/95	85.1/89.6/95.0	85.4/90.7/95.7	89.9/93.1/96.4
10	0.1	$A^{i,3,1,\sigma}$	85/90/95	85.4/90.1/96.0	85.4/90.2/94.6	90.1/93.6/97.0
15	0.1	$A^{i,3,1,\sigma}$	85/90/95	84.1/89.6/94.7	86.0/90.5/95.0	88.9/92.9/96.5
30	0.1	$A^{i,3,1,\sigma}$	85/90/95	85.4/90.3/94.9	85.3/90.1/95.3	88.9/93.4/96.5
10	0.1	$A^{i,3,2,\sigma}$	85/90/95	84.6/90.5/95.1	86.5/91.0/95.3	89.9/93.4/96.3
15	0.1	$A^{i,3,2,\sigma}$	85/90/95	85.2/90.2/95.1	86.2/89.8/95.3	89.8/93.1/96.2
30	0.1	$A^{i,3,2,\sigma}$	85/90/95	85.7/89.6/95.0	85.1/90.6/95.5	90.9/93.2/96.6
10	0.6	$A^{i,1,1,\sigma}$	85/90/95	82.4/87.7/93.9	81.6/87.3/93.6	87.1/91.2/95.5
15	0.6	$A^{i,1,1,\sigma}$	85/90/95	79.9/85.7/92.7	80.7/86.4/92.9	85.2/90.2/94.6
30	0.6	$A^{i,1,1,\sigma}$	85/90/95	79.4/85.5/92.4	78.7/84.8/92.3	82.8/87.6/92.9
10	0.6	$A^{i,1,2,\sigma}$	85/90/95	81.5/87.7/93.8	82.0/88.6/93.8	88.1/92.1/96.0
15	0.6	$A^{i,1,2,\sigma}$	85/90/95	81.9/86.8/93.1	81.0/87.1/93.2	86.3/90.5/94.7
30	0.6	$A^{i,1,2,\sigma}$	85/90/95	80.0/85.7/91.9	80.9/85.6/92.1	85.2/87.6/93.9
10	0.6	$A^{i,3,1,\sigma}$	85/90/95	83.0/88.7/94.7	84.2/88.8/94.2	88.1/91.6/96.0
15	0.6	$A^{i,3,1,\sigma}$	85/90/95	81.9/88.5/93.5	80.9/87.2/93.8	86.0/90.5/95.1
30	0.6	$A^{i,3,1,\sigma}$	85/90/95	80.2/86.7/93.1	80.0/86.3/92.8	85.0/89.5/94.0
10	0.6	$A^{i,3,2,\sigma}$	85/90/95	84.3/89.7/94.4	84.2/89.0/94.9	87.4/92.5/96.2
15	0.6	$A^{i,3,2,\sigma}$	85/90/95	81.5/86.8/93.5	81.6/87.2/94.0	86.2/89.7/95.2
30	0.6	$A^{i,3,2,\sigma}$	85/90/95	81.3/86.6/92.4	81.8/86.7/92.4	85.8/89.2/93.2

Note. Notably, the Ornstein-Uhlenbeck processes $(i=3)$ do not fulfil the assumptions necessary for application of the Gaussian kinematic formula.

markers were placed onto identifiable skin locations on upper and lower volunteers' legs by an experienced technician according to the modified Helen Hayes marker set (Davis et al., 1991) described in the VCM protocol (Vicon, Oxford Metrics, London, UK). Eight cameras recorded the position of the markers and from their motions, a moving orthogonal frame $E_u(t) \in \mathrm{SO}(3)$describing the rotation of the upper leg w.r.t. the laboratory's fixed coordinate system

was determined, and one for the lower leg, $E_l(t) \in \mathrm{SO}(3)$, each of which was aligned near $I_{3\times3}$when the subject stood straight. As is common practice in clinical settings, subjects walked along a predefined 10-m straight path at comfortable speed. For each of the following four sessions (A, B, C, D), for each subject a sample of $N \approx 12$(for details on N, see Table 2) repeated walks have been conducted and for every walk a single gait cycle $\gamma(t) = E_u(t)^T E_l(t)$about half way through has been recorded, representing the motion of the upper leg w.r.t. the lower leg. The resulting curves $\gamma(t)$are reported in the Euler angle parametrisation within the VCM protocol, compare Rivest (2005) for a detailed exposition. After each walk, the volunteers stopped shortly and started again for the next 10-m walk. Thus, by design the assumption of independence of recorded gait cycles is satisfied.

The study consists of four sessions, each giving, as described above, a sample of walks for the left leg of each volunteer. Between samples A and B, the markers were detached and placed again by the same technician following the same standard protocol. Hence, the difference between these samples reflects the challenge of repeated reproducibility of gait patterns under clinical conditions. Before conducting the two sessions, C and D markers were again replaced and the volunteers fulfilled a task of 15 min kneeling prior to data collection of session C and yet another 15 min kneeling prior to session D. This allows to study the effect of kneeling and prolonged kneeling on gait patterns. Table 3 gives an overview of the four sessions conducted. Sessions A and B have already been reported in Telschow et al. (2020).

5.2 Statistical analysis using SCTs

We assume that the samples of relative rotation curves $t \mapsto (E_u^X(t))^T E_l^X(t)$and $t \mapsto (E_u^Y(t))^T E_l^Y(t)$for sessions X and Y are drawn from GP models, and we aim to test whether there is a difference in the respective centre curves $\gamma_0^X$and γ_0^Y. The assumption can be justified as follows. For sample X, say, the VICON software computes the orthonormal frames $E_u^X(t)$, $E_l^X(t) \in \mathrm{SO}(3)$at each time point t. Marker wobbling due to soft tissue effects during movement and imprecision in the recording device imply that the orthonormal frames for the two limbs are perturbed by random rotations $F_u(t)$, $F_l(t) \in \mathrm{SO}(3)$. We assume that the random rotations are given by $F_u(t) = \mathrm{Exp}(\imath(\epsilon_u(t)))$and $F_u(t) = \mathrm{Exp}(\imath(\epsilon_l(t)))$with $\epsilon_l$and ϵ_uGaussian processes with zero-mean and variances small compared to $\pi/2$. The latter assumption is reasonable, since random errors due to soft tissue effects and imprecision in the recording device are very unlikely to rotate the orthonormal frames by large angles. Moreover, we assume that the sample paths are in $\mathcal{C}^2(\mathbb{R}^3)$. Therefore, the orthonormal frames can be modelled as $E_{u,0}^X(t)F_u(t)$and $E_{l,0}^X(t)F_l(t)$with $E_{u,0}^X$, $E_{l,0}^X \in \mathrm{SO}(3)$being the true unobserved orthonormal frames and the resulting model for the final output received from the proprietary software is

$$\left(F_u^X(t)\right)^T \left(E_{u,0}^X(t)\right)^T E_{l,0}^X(t)F_l^X(t) = \left(F_u^X(t)\right)^T \gamma_0^X(t)F_l^X(t) \approx \gamma_0^X(t)\mathrm{Exp}\left(\imath(\tilde{\epsilon}(t))\right)$$

with $\gamma_0^X(t) = (E_{u,0}^X)^T E_{l,0}^X \in \mathrm{SO}(3)$and $\tilde{\epsilon}$a Gaussian process with values in $\mathbb{R}^3$having the same properties as $\epsilon_l$and ϵ_u. The approximation of the two-sided GP model by a one-sided GP model is justified by Telschow et al. (2020, Theorem 2) and used because it is easier to derive approximate SCTs using the GKF in this model. Before we can compare the SCTs for the centre curves of two sessions X and Y, we need to estimate the nuisance effects due to slightly different

Table 2. Reporting the quartiles of numbers of processed walks (gait cycles) of volunteers for each of the four sessions from Table 3

	0%	25%	50%	75%	100%
A	11.00	12.00	12.00	13.00	14.00
B	12.00	12.00	13.00	13.25	14.00
C	9.00	11.75	12.00	12.25	14.00
D	9.00	11.00	12.00	12.25	13.00

Table 3. Experiments conducted

Session	Explanation
A	No intervention, walks
B	No intervention but marker replacement, walks
C	Marker replacement, 15 min of moderate kneeling, walks
D	No marker replacement, another 15 min of prolonged kneeling, walks

Table 4. Reporting p-values (significant in bold face) obtained from the permutation test in Telschow et al. (2020, Test 2.11 in the version of Remark 2.12) correcting for sample-specific group action

Vol	A vs. C	B vs. C	A vs. D	B vs. D
1	0.204	0.158	**0.029**	0.127
2	**0.046**	**0.002**	**0.0**	**0.0**
3	0.872	0.307	0.191	0.311
4	**0.001**	**0.001**	**0.0**	**0.0**
5	0.214	0.735	0.559	0.355
6	**0.0**	**0.0**	**0.001**	**0.008**
7	**0.0**	**0.0**	**0.027**	**0.042**
8	0.467	0.705	0.102	0.149

experimental effects between these sessions caused by marker replacement and different walking speeds.

Again the design of the VICON system implies that replacing markers between two sessions X and Y can result in fixed and different rotations of the constructed orthogonal frames for the upper and lower leg, conveyed by suitable $P, Q \in \mathrm{SO}(3)$such that $E^Y_{u,0}(t) = E^X_{u,0}(t)P^T$and $E^Y_{l,0}(t) = E^X_{l,0}(t)Q$, compare also Rivest (2005, Section 4). Hence, even if the underlying kinematic of the knee movement is identical, the imprecision of marker placement causes a distortion of the centre curves $\gamma^X_0(t)$and $\gamma^Y_0(t)$between sessions given by $\gamma^y_0(t) = P\gamma^X_0(t)Q^T$. This effect can be seen in Figure 1 from Telschow et al. (2020). Estimation of P and Q and temporal alignment of the sample mean curves for two sessions has been done as detailed in Telschow et al. (2020) and Telschow (2016). While the estimation of P and Q could also have been done using the spherical regression technique for rotation matrices, c.f. Prentice (1989) and Rivest and Chang (2006), applied to the sample mean curves of different sessions, the benefit of the approach taken in Telschow et al. (2020) is that it is non-iterative and therefore the estimates can be integrated into the permutation test from Telschow et al. (2020, Test 2.11). Since this global test is not able to locate changes between gait patterns, we identify such changes between two sessions by computing for each sample the SCT of the centre curve and afterwards use the estimated transformations for the temporal alignment and the transformation for removing of the marker placement to find time points where the tubes do not overlap. Simple algebra shows that rejection of $t \in I$, if the confidence tubes at t do not intersect, is a test controlling the family-wise error rate at level at least $1 - (1 - \alpha)^2$, i.e. at level $\approx 0.9$for 0.95-SCTs. However, in general this is a very conservative bound. Here, it is important that the constructed SCTs are equivariant with respect to the group action by $\mathcal{S}$as shown in Theorem 3.6, since otherwise the comparison between two sessions, i.e. the areas of non-overlap, depends on whether we align Y to X or X to Y using the estimated gait similarity. Note that the estimation of the gait similarity between two sessions in Telschow et al. (2020) does not depend on whether we align Y to X or X to Y in the sense that the resulting estimated gait similarities are inverse to each other. The pipeline for the statistical analysis is visualised in Figure 1, and the equivariance property of the SCTs is represented there by the fact that for the resulting SCT it does not depend on whether we align session X to Y and then compute the SCT or compute first the SCT and then apply the gait similarity to obtain the SCT which can be compared to the SCT of the template session.

Table 5. Summarizing the gait events where gait patterns changed such that 0.95 confidence tubes no longer overlap. The abbreviations are explained in Figure 2 0.95

Vol.	A vs. C	B vs. C	A vs. D	B vs. D	Gender	Age group
1				MS	M	20–30
2	HC	TS, HC, HO–TO	TS,HC,TO	TS, HC, HO–TO, MF	M	50–60
3			HC		F	20–30
4			TS	TS	F	50–60
5					M	20–30
6	TO	HO		HO	M	50–60
7		HC			F	20–30
8					F	50–60

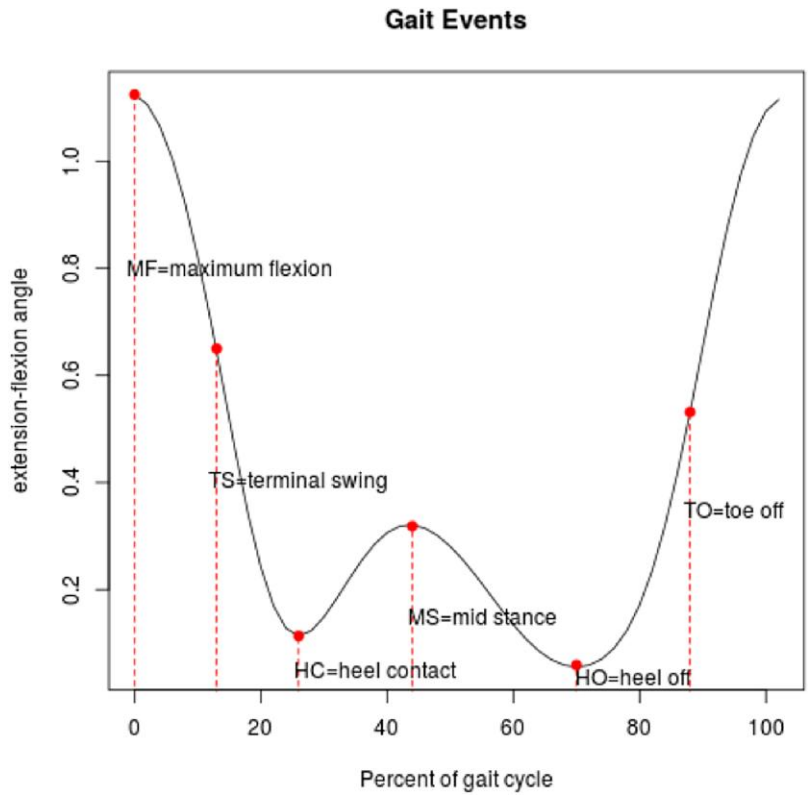

Figure 2. Depicting standard naming convention for gait events with respect to the flexion–extension angle.

5.3 Results

In Table 4, we report the results of the permutation test from Telschow et al. (2020, Test 2.11) which compensates for the variability of estimating the sample-specific group actions, removing the marker replacement effect. If we were not to correct for sample-specific group action, we would detect significant changes of gait for 6 out of the 8 volunteers, even for 'A vs. B', where nothing changed but marker placement, cf. Telschow et al. (2020, Table 2). In Table 4, we see significant (often highly significant) changes of gait of Volunteers 2, 4, 6, and 7 after each of the kneeling tasks. Volunteers 3, 5, and 8 show no changes. Remarkably, these findings are consistent over marker replacement ('A vs. *' and 'B vs. *') and only for Volunteer 1 the picture is unclear.

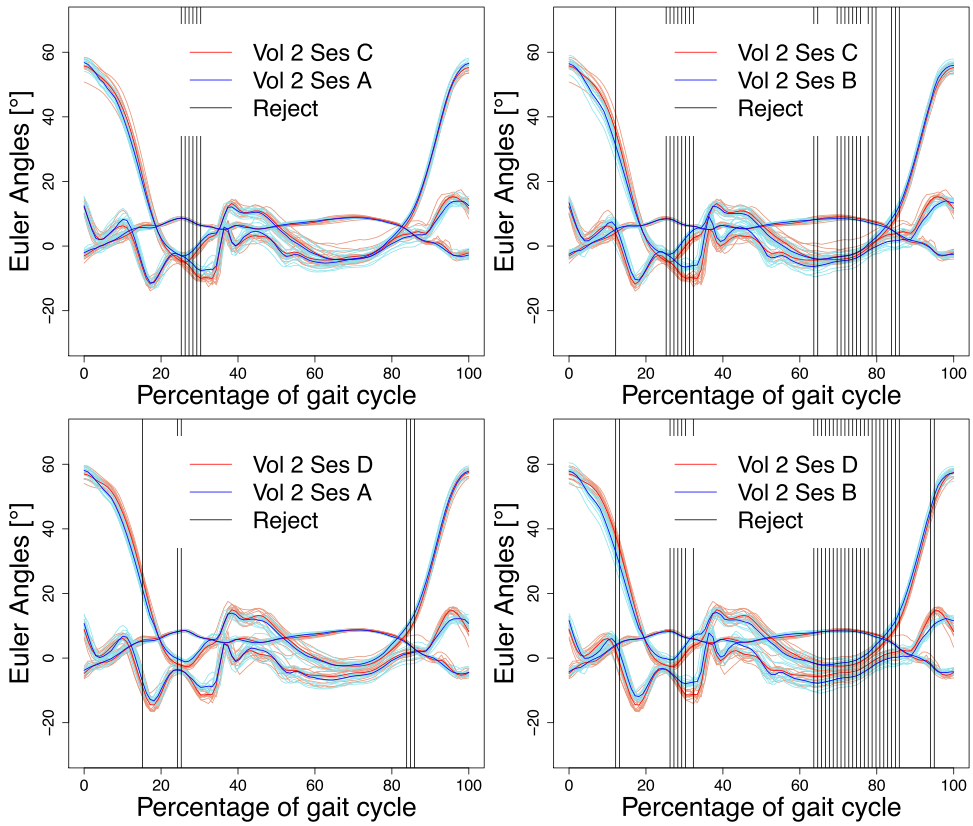

Figure 3. Depicting for Volunteer 2 all three Euler angles of sampled gait curves for each of two different sessions. Point-wise extrinsic mean curves are fat and vertical lines indicate loci of non-overlapping simultaneous 0.05confidence tubes in $SO(3)$. The largely varying curves are flexion–extension angles, cf. Figure 2, the middle curves with least variation are abduction–adduction and the bottom ones are internal–external angles.

In Table 5, we report the specific loci where $1 - \alpha = 0.95$confidence tubes no longer overlap, using standard naming convention (e.g. Rodgers, 1995), as illustrated in Figure 2. Employing Euler angles, which are popular in the field, as a local chart of $SO(3)$, the corresponding curves and specific loci of non-overlapping simultaneous confidence tubes are shown exemplary in Figure 3 for Volunteer 2 and in Figure 4 for Volunteer 6. Notably, non-overlapping confidence tubes have been determined in $SO(3)$and not in chart coordinates so that the chart representations only serve as an approximate visualisation of the real situation which we cannot visualize. The other volunteers' (1, 3, 4, and 7) curves with loci of non-overlapping confidence tubes are shown in the Appendix in Figure A1. Again, we see that Volunteers 5 and 8 feature no changes in gait pattern. Volunteer 7 reported physical pain after post-kneeling walking. Indeed, high variation in gait patterns corresponding to session D (red, in the left two displays of the bottom row in Figure A1) widened the corresponding confidence tubes such that changes of gait in session D were not detected.

Combining Tables 4 and 5 and taking into account age and gender, we see that older age (volunteers with even numbers belong to age group 50–60) favours a kneeling effect over young age (volunteers with odd numbers belong to age group 20–30). As a surprise, the effect seems to be overall stronger for males. Having established a tool chain to study such effects, this experiment warrants larger studies.

6 Discussion

In conjunction with the permutation test and estimation of marker replacement effects from Telschow et al. (2020), with the test for simultaneous non-overlapping confidence tubes presented

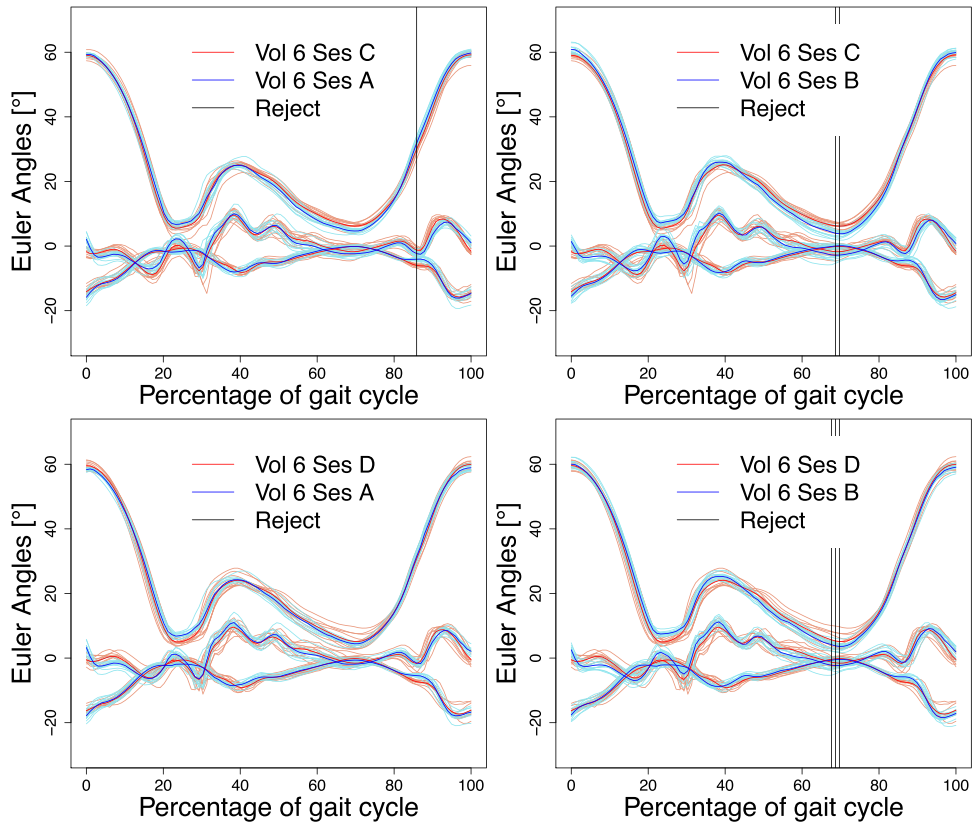

Figure 4. Depicting with notation from Figure 3 for Volunteer 6 all three Euler angles of sampled gait curves for each of two different sessions with point-wise extrinsic mean curves and loci of non-overlapping simultaneous 0.05confidence tubes in SO(3).

in this paper, we have developed a tool chain that can be used in clinical practice to assess changes of gait patterns and localise these. These are no longer based on (single) Euler angle representations, as are often used in the field, but take advantage of a Gaussian perturbation model defined in the Lie group of three-dimensional rotations. Due to the conservation of moment, gait curves of relative rotations of the knee joints are naturally smooth, densely sampled and their variation between observed time points as well as over repeated walks is moderate. Hence, approximations via Gaussian perturbation models and the GKF are rather accurate, in theory as well as in practice.

In this study, with a small number of participants and a small number of repeated walks, we see that short kneeling tasks tend to affect gait patterns and it seems that older age and, possibly, male gender, favour this effect. We have made sure that this effect has not been caused by different marker placements. While specific loci of gait change depend on individuals, changes seem to occur least at local maxima of dominating flexion–extension, namely at MF and MS.

Future research involves building simultaneous conference tubes for a proper 'difference', e.g. $(\gamma_0^X)^T\gamma_0^Y$, of mean curves of two samples of curves in SO(3), since we expect them to be even more powerful in identifying locations of significant differences in gait patterns. This, however, comes with the additional challenge of incorporating the sample-specific group action caused by different walking speeds and marker replacement, which we solved here by the equivariance property of the SCTs.

Furthermore, we believe that our results derived for SO(3)generalise to general connected Lie groups, in particular to products of SO(3)with itself and with the Euclidean motion group. Providing SCTs for these Lie groups would be helpful for biomechanical analysis of more complicated joints (e.g. Rivest et al., 2008 for ankle motion) and in motion analysis of *kinematic chains* of entire limbs (e.g. Laitenberger et al., 2015) and their design for humanoid robots (e.g. Ude et al., 2004).

Acknowledgments

We want to thank the anonymous referees for their careful reading and helpful suggestions. Both helped to improve the readability of our manuscript substantially.

Conflict of interest: The authors certify that they have no affiliations with or involvement in any organization or entity with any financial interest (such as honoraria; educational grants; participation in speakers' bureaus; membership, employment, consultancies, stock ownership, or other equity interest; and expert testimony or patent-licensing arrangements), or non-financial interest (such as personal or professional relationships, affiliations, knowledge or beliefs) in the subject matter or materials discussed in this manuscript.

Funding

F.J.E.T. is funded by the Deutsche Forschungsgemeinschaft (DFG) under Excellence Strategy The Berlin Mathematics Research Center MATH+ (EXC-2046/1, project ID:390685689). F.J.E.T. and S.F.H. gratefully acknowledge the support from DFG HU 1575/4 and 1575/7, the Niedersachsen Vorab of the Volkswagen Foundation and DFG GRK 2088.

Data availability

An R-package containing the presented methods is available under www.stochastik.math.uni-goettingen.de/KneeMotionAnalytics.

Appendix A. Visualisations of non-overlapping SCTs

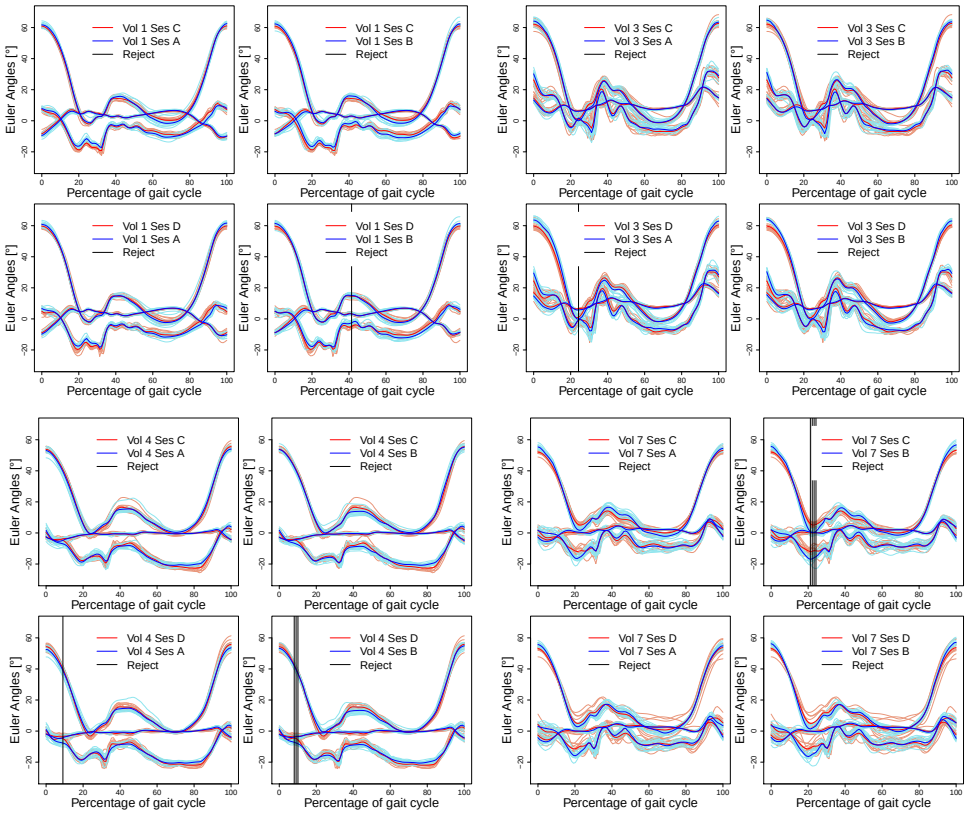

Figure A1. Results of the SCT test for Volunteers 1, 3, 4, and 7. The presentation is the same as in Figure 3. We show all three Euler angles of the sampled gait curves for each of two different sessions together with the point-wise extrinsic mean curves and loci of non-overlapping simultaneous 0.05confidence tubes in SO(3).

Appendix B. Proofs

Proof of Theorem 3.4. The following statements are equivalent, since $\mathfrak{L}$is a bijection:

$$\begin{aligned}\gamma_0(t) \in \hat{\gamma}_N(t)\mathrm{Exp}\big(\iota\big(\mathcal{V}_\alpha(\gamma_1, \ldots, \gamma_N; t)\big)\big) &\Leftrightarrow \hat{\gamma}_N(t)^{-1}\gamma_0(t) \\ &\quad \in \mathrm{Exp}\big(\iota\big(\mathcal{V}_\alpha(\gamma_1, \ldots, \gamma_N; t)\big)\big) \\ &\Leftrightarrow x_t^N \in \mathfrak{L} \\ &\quad \big(\mathrm{Exp}\big(\iota\big(\mathcal{V}_\alpha(\gamma_1, \ldots, \gamma_N; t)\big)\big)\big) \\ &\Leftrightarrow x_t^N \in \mathcal{V}_\alpha(\gamma_1, \ldots, \gamma_N; t).\end{aligned}$$

To see the last equivalence note that the direction '$\Rightarrow$' holds, since by construction

$$\mathfrak{L}\big(\mathrm{Exp}\big(\iota\big(\mathcal{V}_\alpha(\gamma_1, \ldots, \gamma_N; t)\big)\big)\big) \subseteq \mathcal{V}_\alpha(\gamma_1, \ldots, \gamma_N; t).$$

The direction '$\Leftarrow$' holds because $x_t^N$is contained in the image of $\mathfrak{L}$. Hence, if $x_t^N \in \mathcal{V}_\alpha(\gamma_1, \ldots, \gamma_N; t)$it follows that $x_t^N \in \mathfrak{L}(\mathrm{Exp}(\iota(\mathcal{V}_\alpha(\gamma_1, \ldots, \gamma_N; t))))$. The proof is finished, since by the definition of $\hat{h}_{\gamma_0,N,\alpha}$the probability that the last equivalence holds simultaneously for all $t \in I$is at least $1 - \alpha$. □

Proof of Theorem 3.6. With the intrinisic residuals for each of the samples:

$$x_t^{N,n} = \mathfrak{L}\big(\hat{\gamma}_N^T(t)\gamma_n(t)\big) \quad \text{and} \quad y_t^{N,n} = \mathfrak{L}\big(\hat{\eta}_N^T(t)\eta_n(t)\big),$$

due to equivariance, $\hat{\eta}_N = \psi \circ \hat{\gamma}_N \circ \phi$, setting $\psi(R) = P_\psi R Q_\psi$with R, P_ψ, $Q_\psi \in \mathrm{SO}(3)$, we have

$$\begin{aligned}y_t^{N,n} &= \iota^{-1} \circ \mathrm{Log}\Big(Q_{\hat{\psi}_N}^T\big(\phi(t)\big)\gamma_n\big(\phi(t)\big)Q_\psi\Big) \\ &= \pm\iota^{-1}\Big(Q_\psi^T\mathrm{Log}\big(\hat{\gamma}_N^T\big(\phi(t)\big)\gamma_n\big(\phi(t)\big)\big)Q_\psi\Big) \\ &= \pm Q_\psi\iota^{-1} \circ \mathrm{Log}\big(\hat{\gamma}_N^T\big(\phi(t)\big)\gamma_n\big(\phi(t)\big)\big) \\ &= \pm Q_\psi x_{\phi(t)}^{N,n}.\end{aligned}$$

Here, the second equality is due to the power series expansion of the matrix logarithm and the observation that different extensions of the matrix logarithm to the cut locus of $I_{3\times3}$differ only by their sign; the third equality is due to equation (1). Moreover, by a similar argument for $x_t^N = \mathfrak{L}(\hat{\gamma}_N^T(t)\gamma_0(t))$and $y_t^N = \mathfrak{L}(\hat{\eta}_N^T(t)\eta_0(t))$we obtain $y_t^N = \pm Q_\psi x_{\phi(t)}^N$, yielding

$$\hat{S}_t^{y,N} = Q_\psi \hat{S}_{\phi(t)}^x Q_\psi^T, \quad \hat{H}_t^{y,N} = \hat{H}_{\phi(t)}^x \quad \text{and} \quad \hat{h}_{\gamma_0,N,\beta} = \hat{h}_{\eta,N,\beta}.$$

This implies $\mathcal{V}_\beta((\eta_1, \ldots, \eta_N); t) = Q_\psi\mathcal{V}_\beta(\gamma_1, \ldots, \gamma_N; \phi(t))$, yielding the assertion. □

Proof of Theorem 3.7. Recall that the generating Gaussian process $a_t$can be considered to be a process in $\mathfrak{so}(3)$by defining $A_t = \iota(a_t)$. Consider samples

$\gamma_1, \ldots, \gamma_N$with fixed $N \in \mathbb{N}$of a GP model $\gamma_0 \mathrm{Exp}(A_t)$with $a_t = \imath^{-1} \circ A_t$, $\max_{t\in I} \|a_t\| = \mathcal{O}_p(\sigma)$and $\sigma \to 0$, and let $\hat{\gamma}_N(t) \in E_N(t)$be a measurable selection of PEMs. Then for each $t \in I$, taking $x_t^N \in \mathbb{R}^3$from Definition 3.3 and $X_t^N = \imath(x_t^N)$, we have that $\hat{\gamma}_N(t) = \gamma_0 \mathrm{Exp}(X_t^N)$. Making use of the fact

$$\left(\imath\left(\frac{x}{\|x\|}\right)\right)^2 = \frac{xx^T}{\|x\|^2} - I_{3\times 3}, \tag{B1}$$

the property $\mathrm{trace}(\imath(c)^T \imath(d)) = 2c^T d$for all $c, d \in \mathbb{R}^3$and the Rodriguez formula (2), we have for each $t \in I$that X_t^Nmaximises

$$\begin{aligned}
&\frac{1}{N}\sum_{n=1}^{N} \mathrm{trace}\left(\hat{\gamma}_N^T(t)\gamma_0(t)\mathrm{Exp}\left(A_t^n\right)\right) \\
&= \mathrm{trace}\left(\left(I_{3\times 3} + \imath\left(x_t^N\right)\mathrm{sinc}\left(\left\|X_t^N\right\|_F\right) + \frac{1-\cos\left(\left\|X_t^N\right\|_F\right)}{\left\|X_t^N\right\|_F^2}\imath\left(x_t^N\right)^2\right)^T\right. \\
&\quad \left.\cdot \left(I_{3\times 3} + \imath(\bar{a}_t) + \mathcal{O}_p\left(\sigma^2\right)\right)\right) \\
&= 3 + \mathrm{trace} \\
&\left(\imath\left(x_t^N\right)^T \imath(\bar{a}_t)\mathrm{sinc}(\|x_t^M\|) + (1-\cos\left(\|x_t^N\|\right)\left(\imath\left(\frac{x_t^N}{\|x_t^N\|}\right)\right)^2 + \mathcal{O}_p(\sigma_l^2)\right) \\
&= 1 + 2\left({x_t^N}^T \bar{a}_t \mathrm{sinc}(\|x_t^N\|) + \cos\left(\|x_t^N\|\right)\right) + \mathcal{O}_p(\sigma^2).
\end{aligned}$$

Note that the $\mathcal{O}_p(\sigma^2)$is indeed uniform in $t \in I$.

Writing $x_t^N = re$with a unit vector e and length $0 \le r \le \pi$, the first two summands above are maximised in x_t^Nif

$$s \sin(r) + \cos(r)$$

is maximal under the side condition $-\|\bar{a}_t\| \le s = e^T \bar{a}_t \le \|\bar{a}_t\|$. Hence, for $0 \le r < \pi$choose the maximising $s = \|\bar{a}_t\|$(as large as possible) and hence $r = \arctan\left(\|\bar{a}_t\|\right) \in (0, \pi/2)$($r = \pi$is no option). In consequence we have that

$$x_t^N = \bar{a}_t \frac{\arctan\|\bar{a}_t\|}{\|\bar{a}_t\|} + \mathcal{O}_p\left(\sigma^2\right) = \bar{a}_t + \mathcal{O}_p\left(\sigma^2\right).$$

This is the first claimed identity in equation (10).

To establish the second identity, consider the Taylor expansion

$$\begin{aligned}
x_t^{N,n} &= \mathfrak{L}\left(\hat{\gamma}_N^T(t)\gamma_n(t)\right) = \imath^{-1} \circ \mathrm{Log}\left(\mathrm{Exp}\left(-\imath(\bar{a}_t) + \mathcal{O}_p\left(\sigma^2\right)\right)\mathrm{Exp}\left(\imath\left(a_t^n\right)\right)\right) \\
&= a_t^n - \bar{a}_t^N + \mathcal{O}_p(\sigma^2)
\end{aligned}$$

which is not valid for $\|a_t^n - x_t^N\| \ge \pi$, cf. Chirikjian (2000, p. 121). The probability of which, however, is $\mathcal{O}(\sigma^2)$, uniformly over $t \in I$, yielding the second assertion. □

Proof of Corollary 3.8. Recall the definitions

$$H_t^a = N(\bar{a}_t)^T \left(S_t^a\right)^{-1} \bar{a}_t \quad \text{and} \quad \tilde{H}_t^x = N\left(x_t^N\right)^T \left(\hat{S}_t^x\right)^{-1} x_t^N.$$

By virtue of Theorem 3.7 we obtain

$$\hat{S}_t^x = S_t^a + Z_t$$

with $\max_t \|Z_t\|_F = \mathcal{O}_p(\sigma_l^3)$. Using Henderson and Searle (1981, p. 58, equation (24)) yields

$$\begin{aligned}\frac{1}{N}\hat{H}_t^x &= (x_t^N)^T (S_t^a + Z_t)^{-1} x_t^N \\ &= \left(x_t^N\right)^T (S_t^a)^{-1} x_t^N - (x_t^N)^T \left(S_t^a\right)^{-1} \\ &\quad Z_t \left(I_{3\times 3} + \left(S_t^a\right)^{-1} Z_t\right)^{-1} \left(S_t^a\right)^{-1} x_t^N.\end{aligned}$$

From the assumption $\text{var}[a_t^n] = \sigma^2 \Sigma_t$we have that $\max_{t\in I} \|(S_t^a)^{-1}\|_F = \mathcal{O}_p(\sigma^{-2})$. Thus, we obtain

$$\left(x_t^N\right)^T \left(S_t^a\right)^{-1} x_t^N = \frac{1}{N} H_t^a + \mathcal{O}_p(\sigma)$$

by Theorem 3.7. Moreover, we obtain that $\max_{t\in I} \|(S_t^a)^{-1} Z_t\|_F = \mathcal{O}_p(\sigma)$implying $(S_t^a)^{-1} Z_t \xrightarrow{\mathbb{P}} 0$uniformly over $t \in I$. In consequence, on $U = \{\|(S_t^a)^{-1} Z_t\|_F < 1\}$we have the Von Neumann series

$$\left(I_{3\times 3} + \left(S_t^a\right)^{-1} Z_t\right)^{-1} = \sum_{j=0}^{\infty} (-1)^j \left(\left(S_t^a\right)^{-1} Z_t\right)^j$$

showing at once

$$\left(x_t^N\right)^T \left(S_t^a\right)^{-1} Z_t \left(I_{3\times 3} + \left(S_t^a\right)^{-1} Z_t\right)^{-1} \left(S_t^a\right)^{-1} x_t^N = \mathcal{O}_p(\sigma).$$

Since $\mathbb{P}\{U\} = 1 - \mathcal{O}(\sigma)$, this completes the proof. □

References

Bhattacharya R., & Patrangenaru V. (2003). Large sample theory of intrinsic and extrinsic sample means on manifolds. *The Annals of Statistics*, *31*(1), 1–29. https://doi.org/10.1214/aos/1046294456

Chirikjian G. S. (2000). *Engineering applications of noncommutative harmonic analysis: With emphasis on rotation and motion groups*. CRC Press.

Coggon D., Croft P., Kellingray S., Barrett D., McLaren M., & Cooper C. (2000). Occupational physical activities and osteoarthritis of the knee. *Arthritis & Rheumatism*, *43*(7), 1443–1449. https://doi.org/10.1002/1529-0131(200007)43:7<1443::AID-ANR5>3.0.CO;2-1

Cooper C., McAlindon T., Coggon D., Egger P., & Dieppe P. (1994). Occupational activity and osteoarthritis of the knee. *Annals of the Rheumatic Diseases*, *53*(2), 90–93. https://doi.org/10.1136/ard.53.2.90

Davis R. B., Ounpuu S., Tyburski D., & Gage J. R. (1991). A gait analysis data collection and reduction technique. *Human Movement Science*, *10*(5), 575–587. https://doi.org/10.1016/0167-9457(91)90046-Z

Delval A., Salleron J., Bourriez J.-L., Bleuse S., Moreau C., Krystkowiak P., Luc Defebvre P. D., & Duhamel A. (2008). Kinematic angular parameters in PD: Reliability of joint angle curves and comparison with healthy subjects. *Gait and Posture*, *28*(3), 495–501. https://doi.org/10.1016/j.gaitpost.2008.03.003

Duhamel A., Bourriez J., Devos P., Krystkowiak P., Destee A., Derambure P., & Defebvre L. (2004). Statistical tools for clinical gait analysis. *Gait & Posture*, *20*(2), 204–212. https://doi.org/10.1016/j.gaitpost.2003.09.010

Gaudreault N., Hagemeister N., Poitras S., & de Guise J. A. (2013). Comparison of knee gait kinematics of workers exposed to knee straining posture to those of non-knee straining workers. *Gait & Posture*, *38*(2), 187–191. https://doi.org/10.1016/j.gaitpost.2012.11.004

Henderson H. V., & Searle S. R. (1981). On deriving the inverse of a sum of matrices. *Siam Review*, *23*(1), 53–60. https://doi.org/10.1137/1023004

Iacus S. M. (2009). *Simulation and inference for stochastic differential equations: With R examples*. Springer Science & Business Media.

Kadaba M., Ramakrishnan H., Wootten M., Gainey J., Gorton G., & Cochran G. (1989). Repeatability of kinematic, kinetic, and electromyographic data in normal adult gait. *Journal of Orthopaedic Research*, *7*(6), 849–860. https://doi.org/10.1002/jor.1100070611

Kajaks T., & Costigan P. (2015). The effect of sustained static kneeling on kinetic and kinematic knee joint gait parameters. *Applied Ergonomics*, *46*(Part A), 224–230. https://doi.org/10.1016/j.apergo.2014.08.011

Laitenberger M., Raison M., Périé D., & Begon M. (2015). Refinement of the upper limb joint kinematics and dynamics using a subject-specific closed-loop forearm model. *Multibody System Dynamics*, *33*(4), 413–438. https://doi.org/10.1007/s11044-014-9421-z

McGinley J. L., Baker R., Wolfe R., & Morris M. E. (2009). The reliability of three-dimensional kinematic gait measurements: A systematic review. *Gait & Posture*, *29*(3), 360–369. https://doi.org/10.1016/j.gaitpost.2008.09.003

Mecke K. R., & Stoyan D. (2000). *Statistical physics and spatial statistics: The art of analyzing and modeling spatial structures and pattern formation* (Vol. *554*). Springer Science & Business Media.

Noehren B., Manal K., & Davis I. (2010). Improving between-day kinematic reliability using a marker placement device. *Journal of Orthopaedic Research*, *28*(11), 1405–1410. https://doi.org/10.1002/jor.21172

Prentice M. J. (1989). Spherical regression on matched pairs of orientation statistics. *Journal of the Royal Statistical Society: Series B (Methodological)*, *51*(2), 241–248. https://doi.org/10.1111/j.2517-6161.1989.tb01761.x

Rancourt D., Rivest L.-P., & Asselin J. (2000). Using orientation statistics to investigate variations in human kinematics. *Applied Statistics*, *49*(1), 81–94. https://doi.org/10.1111/1467-9876.00180

Rivest L.-P. (2005). A correction for axis misalignment in the joint angle curves representing knee movement in gait analysis. *Journal of Biomechanics*, *38*(8), 1604–1611. https://doi.org/10.1016/j.jbiomech.2004.07.031

Rivest L.-P., Baillargeon S., & Pierrynowski M. (2008). A directional model for the estimation of the rotation axes of the ankle joint. *Journal of the American Statistical Association*, *103*(483), 1060–1069. https://doi.org/10.1198/016214508000000643

Rivest L.-P., & Chang T. (2006). Regression and correlation for 3×3rotation matrices. *Canadian Journal of Statistics*, *34*(2), 187–202. https://doi.org/10.1002/cjs.5550340201

Rodgers M. M. (1995). Dynamic foot biomechanics. *Journal of Orthopaedic & Sports Physical Therapy*, *21*(6), 306–316. https://www.jospt.org/doi/10.2519/jospt.1995.21.6.306

Røislien J., Skare Ø., Opheim A., & Rennie L. (2012). Evaluating the properties of the coefficient of multiple correlation (CMC) for kinematic gait data. *Journal of Biomechanics*, *45*(11), 2014–2018. https://doi.org/10.1016/j.jbiomech.2012.05.014

Rytter S., Egund N., Jensen L. K., & Bonde J. P. (2009). Occupational kneeling and radiographic tibiofemoral and patellofemoral osteoarthritis. *Journal of Occupational Medicine and Toxicology*, *4*(1), 19. https://doi.org/10.1186/1745-6673-4-19

Rytter S., Jensen L. K., Bonde J. P., Jurik A. G., & Egund N. (2009). Occupational kneeling and meniscal tears: A magnetic resonance imaging study in floor layers. *The Journal of Rheumatology*, *36*(7), 1512–1519. https://doi.org/10.3899/jrheum.081150

Taylor J., Takemura A., & Adler R. J. (2005). Validity of the expected Euler characteristic heuristic. *Annals of Probability*, 33(4), 1362–1396. https://doi.org/10.1214/009117905000000099

Taylor J., & Worsley K. (2008). Random fields of multivariate test statistics, with applications to shape analysis. *The Annals of Statistics*, 36(1), 1–27. https://doi.org/10.1214/009053607000000406

Taylor J. E. (2006). A Gaussian kinematic formula. *The Annals of Probability*, *34*(1), 122–158. https://doi.org/10.1214/009117905000000594

Taylor J. E., & Worsley K. J. (2007). Detecting sparse signals in random fields, with an application to brain mapping. *Journal of the American Statistical Association*, *102*(479), 913–928. https://doi.org/10.1198/016214507000000815

Telschow F. J. E., Pierrynowski M. R., & Huckemann S. F. (2020). Functional inference on rotational curves under sample-specific group actions and identification of human gait. *Scandinavian Journal of Statistics*, *48*(4), 1256–1676. https://doi.org/10.1111/sjos.12488

Telschow F. J. E. (2016). *Equivariant functional shape analysis in SO (3) with applications to gait analysis* [Ph.D. thesis]. Göttingen, Georg-August Universität.

Telschow F. J. E., & Schwartzman A. (2022). Simultaneous confidence bands for functional data using the Gaussian kinematic formula. *Journal of Statistical Planning and Inference*, *216*, 70–94. https://doi.org/10.1016/j.jspi.2021.05.008

Tennant L., Kingston D., Chong H., & Acker S. (2015). The effect of work boots on knee mechanics and the center of pressure at the knee during static kneeling. *Journal of Applied Biomechanics*, *31*(5), 363–369. https://doi.org/10.1123/jab.2014-0276

Tennant L. M., Chong H. C., & Acker S. M. (2018). The effects of a simulated occupational kneeling exposure on squat mechanics and knee joint load during gait. *Ergonomics*, *61*(6), 839–852. https://doi.org/10.1080/00140139.2017.1411529

Ude A., Atkeson C. G., & Riley M. (2004). Programming full-body movements for humanoid robots by observation. *Robotics and Autonomous Systems*, *47*(2–3), 93–108. https://doi.org/10.1016/j.robot.2004.03.004

Wilkens K. J., Duong L. V., McGarry M. H., Kim W. C., & Lee T. Q. (2007). Biomechanical effects of kneeling after total knee arthroplasty. *The Journal of Bone and Joint Surgery-American Volume*, *89*(12), 2745–2751. https://doi.org/10.2106/JBJS.E.01201